Article

Not peer-reviewed version

Metabolite Profiling-Based Characterization and Antibacterial Activity of Sea Cucumber *Isostichopus*. sp. *aff. badionotus* from Colombian Caribbean Sea

Manuel E. Taborda-Martínez *, Adriana Rodríguez-Forero, Mitchell Bacho, Fabián Espitia-Almeida, Ericsson Coy-Barrera, Yeray A. Rodríguez-Núñez *

Posted Date: 14 May 2025

doi: 10.20944/preprints202505.1052.v1

Keywords: Sea cucumber; *Isostichopus* spp.; Marine natural products; Metabolite profiling; Molecular networking; Antibacterial activity

Article

Metabolite Profiling-Based Characterization and Antibacterial Activity of Sea Cucumber *Isostichopus*. sp. *aff. badionotus* from Colombian Caribbean Sea

Manuel E. Taborda-Martínez [1,*], Adriana Rodríguez-Forero [1], Mitchell Bacho [2], Fabián Espitia-Almeida [3], Ericsson Coy-Barrera [4] and Yeray A. Rodríguez-Núñez [2,*]

[1] Universidad del Magdalena, Santa Marta 470004, Colombia

[2] Laboratorio de Síntesis y Reactividad de Compuestos Orgánicos, Universidad Andrés Bello, Facultad de Ciencias Exactas, Departamento de Ciencias Químicas, Santiago 8370146, Chile

[3] Centro de Investigaciones en Ciencias de la Vida, Facultad de Ciencias Básicas y Biomédicas, Universidad Simón Bolívar, Barranquilla 080002, Colombia

[4] Bioorganic Chemistry Laboratory, Universidad Militar Nueva Granada, Cajicá 250247, Colombia

* Correspondence: mtaborda@unimagdalena.edu.co (M.E.T.-M.); yeray.rodriguez@unab.cl (Y.A.R.-N.)

Abstract: Background/Objectives: Marine organisms such as sea cucumbers are rich sources of bioactive specialized metabolites with promising pharmaceutical potential, including antibacterial properties. This study aimed to chemically characterize and evaluate the antibacterial activity of the parent methanolic extract and its derived fractions, obtained through sequential liquid–liquid partitioning, from the sea cucumber *Isostichopus* sp. aff. *badionotus* collected from the Colombian Caribbean Sea. **Methods:** The chemical profiles of the extract and fractions were analyzed using ultra-high-performance liquid chromatography coupled to mass spectrometry (UHPLC-MS) and the Global Natural Products Social (GNPS)-based molecular networking platform, enabling dereplication and identification of metabolites. Additionally, extract and fractions were evaluated against eight Gram-positive and Gram-negative bacterial strains. **Results:** The dichloromethane fractions exhibited the highest antibacterial activity against both Gram-positive and Gram-negative bacteria. For the first time, chemical characterization allowed the identification of a series of metabolites present in the extract and fractions. **Conclusion:** This study provides the first report of antibacterial activity in *Isostichopus* sp. *aff. badionotus*, demonstrating that medium-polarity compounds in the dichloromethane fraction exhibited moderate bacterial inhibition, particularly against Gram-positive strains.

Keywords: Sea cucumber; *Isostichopus* spp.; Marine natural products; Metabolite profiling; Molecular networking; Antibacterial activity

1. Introduction

Bacterial drug resistance remains one of the most pressing challenges to global public health, largely driven by the overuse and misuse of antibiotics. This phenomenon results in a marked reduction in the efficacy of conventional treatments and a significant increase in patient morbidity and mortality rates [1]. In response to this urgent threat, searching for new bioactive compounds with antibacterial potential has become a global research priority. Considering this context, natural products have historically been a critical source of therapeutic agents, and marine-derived compounds, in particular, have gained prominence due to their chemical diversity, structural complexity, and unique bioactivity profiles [2]. Marine ecosystems, with their vast and largely unexplored biodiversity, offer promising opportunities for discovering and developing novel antibacterial agents.

 doi:10.20944/preprints202505.1052.v1

Sea cucumbers—marine invertebrates belonging to the Holothuroidea—have attracted significant attention among marine organisms. Distributed in both deep and shallow coastal waters worldwide [3]. Sea cucumbers possess a diverse repertoire of metabolites, likely linked to their detritivorous feeding habits and adaptation to complex ecological niches. In addition to their traditional use as a food source in many cultures, particularly in Asia, sea cucumbers have been the focus of numerous studies investigating their biological properties, including antioxidant [4–6], anti-inflammatory [6,7], anticancer [8,9], and antihypertensive properties [10,11], among others. Furthermore, several studies have reported the antimicrobial potential of different sea cucumber species [4,12–14], highlighting their promise as a natural alternative for combating bacterial resistance. Despite these advances, information regarding the antibacterial activity and chemical composition of certain sea cucumber species, particularly those from the Colombian Caribbean Sea, remains scarce. *Isostichopus* sp. aff. *badionotus* is a species of ecological and commercial importance in this region, yet its specialized (formerly secondary) metabolites and potential bioactivities have not been fully characterized.

In the present study, we aimed to expand the chemical and biological understanding of the *Isostichopus* genus by characterizing the chemical composition of the parent methanol extract and its derived fractions obtained through sequential liquid-liquid partitioning from *Isostichopus* sp. aff. *badionotus*, collected from the coastal waters of northern Colombia. Ultra-high-performance liquid chromatography coupled with mass spectrometry (UHPLC-MS), along with the Global Natural Products Social (GNPS) molecular networking platform, was employed for metabolite profiling. Additionally, we evaluated, for the first time, the antibacterial activity of the extract and fractions against eight Gram-positive and Gram-negative bacterial strains. This integrative approach enabled the identification of metabolites potentially responsible for the observed antibacterial effects and contributed to the growing body of knowledge on marine-derived antibacterial compounds.

2. Results and Discussion

To evaluate the antibacterial potential of *Isostichopus* sp. aff. *badionotus*, specimens were collected from three coastal sites in the Santa Marta Bay (Colombia), and a methanolic (MeOH) crude extract was prepared and subsequently partitioned through liquid-liquid extraction to yield hexane (Hex), dichloromethane (DCM), and butanol (BuOH) fractions. The extract and its fractions were tested against eight clinically relevant bacterial strains using the CLSI broth microdilution method. In parallel, UHPLC-QTOF-MS-based metabolite profiling coupled with GNPS molecular networking was conducted to characterize the specialized metabolites in the fractions and explore potential correlations with observed antibacterial activity.

2.1. Chemical Characterization of Extract and Fractions from Isostichopus sp. aff badionotus.

The UHPLC-QTOF-MS-based chemical characterization aimed to reveal the profile of specialized metabolites present in each extract/fractions and assess the effectiveness of the fractionation strategy. This approach was conducted in both positive and negative ionization modes to ensure comprehensive detection. High-resolution monoisotopic masses, tandem MS/MS fragmentation patterns, and chromatographic retention times were systematically compared against spectral databases including MS-DIAL, MoNA (MassBank of North America), and LipidBlast for accurate compound annotation. This analysis exposed a diverse array of lipid-derived specialized metabolites. In the negative ionization mode, compounds were primarily associated with classes such as lysophosphatidylethanolamines (LPE), lysophosphatidic acids (LPA), lysophosphatidylcholines (LPC), lysophosphatidylserines (LPS), phosphoethanolamines (PE-O), glycerophosphoinositols (LPI), and sulfated sterols (ST). Conversely, positive ionization mode predominantly identified lipids including lysodiacylglycerylcarboxyhydroxymethylcholines (LDGCC), sphingomyelins (SM), LPEs, phosphatidylcholines (PC), and LPCs. Figure 2 depicts representative molecular structures of the major specialized metabolites detected under each ionization condition, with panel A corresponding to those annotated in negative mode and panel B to those in positive mode.

 doi:10.20944/preprints202505.1052.v1

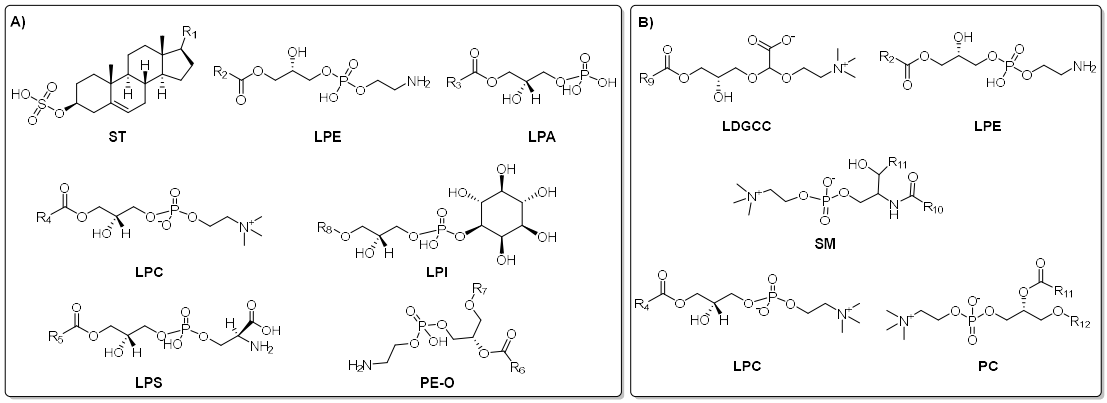

Figure 1. Annotated compound classes in *I.* sp. *aff badionotus* extract and fractions by UHPLC-MS/MS-based analysis. A) Metabolites detected and annotated in negative mode. B) Metabolites detected and annotated in positive mode. Lysophosphatidylethanolamines (LPE), lysophosphatidic acids (LPA), lysophosphatidylcholines (LPC), lysophosphatidylserines (LPS), phosphoethanolamines (PE-O), glycerophosphoinositols (LPI), sulfated sterols (ST), lysodiacylglycerylcarboxyhydroxymethylcholines (LDGCC), sphingomyelins (SM), phosphatidylcholines (PC).

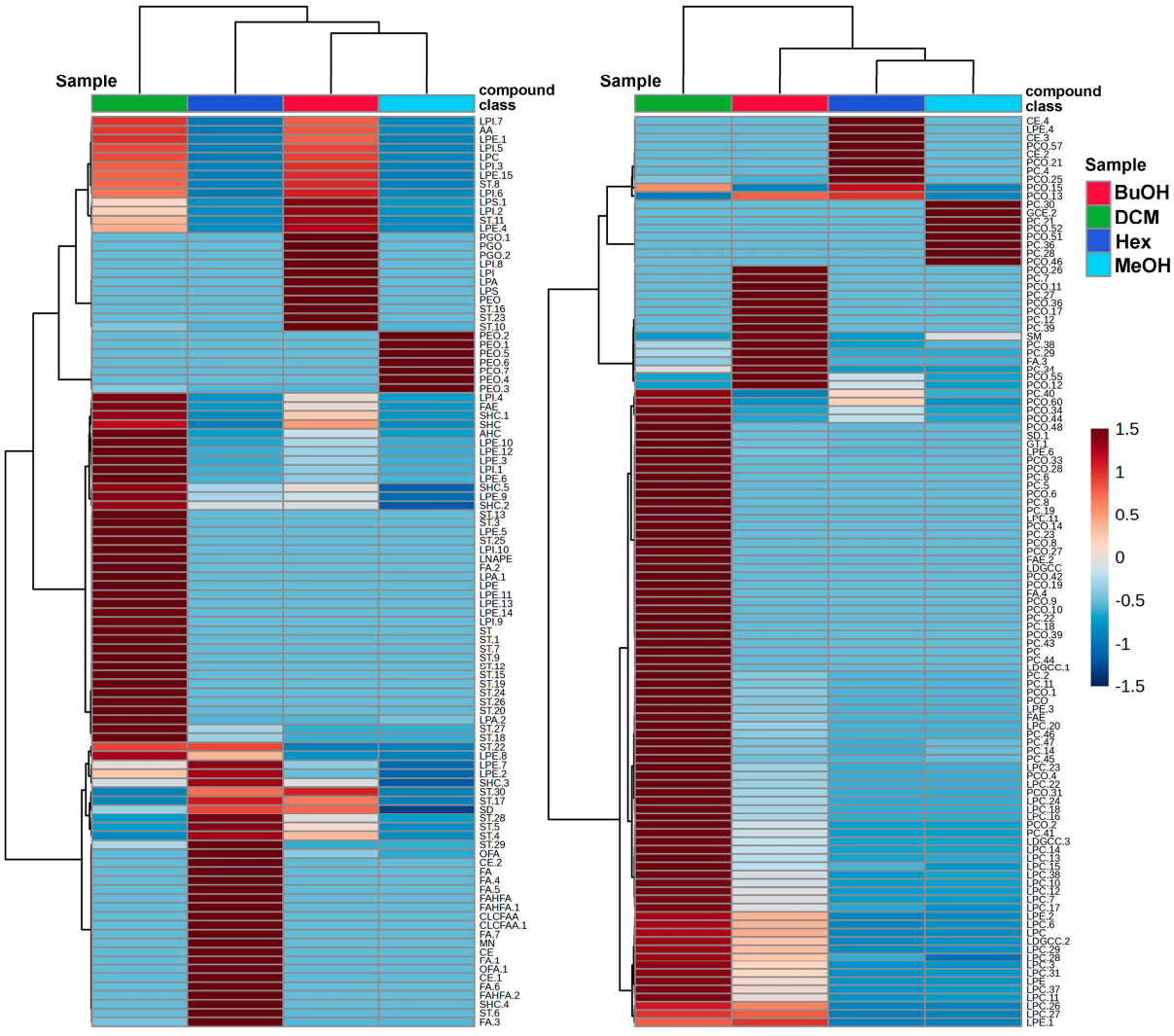

Figure 2. Heat map of the relative abundance of metabolites detected in the methanolic extract (MeOH) and its solvent fractions—hexane (Hex), dichloromethane (DCM), and butanol (BuOH)—of *Isostichopus* sp. aff. *badionotus*. (A) and (B) represent the two subsets of metabolites from negative (A) and positive (B) ion modes,

 doi:10.20944/preprints202505.1052.v1

respectively clustered based on their intensity patterns across the parent extract (MeOH) and its three fractions. The color scale indicates normalized intensity values, with red representing higher abundance and blue lower abundance. Hierarchical clustering highlights distinct chemical profiles among the extract/fractions, reflecting the differential distribution of metabolites according to partitioning. Class compounds are abbreviated according to Figure 1.

The distribution and relative abundance of the annotated metabolites across the different extract and its derived fractions are intuitively visualized in the heat map (Figure 2), which presents two subsets of detected compounds obtained under negative and positive ionization modes (Figure 2A and 2B, respectively). Metabolite intensities were normalized and visualized using a color gradient, with red tones indicating higher abundance and blue tones representing lower abundance. Thus, hierarchical clustering of both subsets and extract/fractions revealed distinct chemical profiles among the fractions, emphasizing the efficiency of the liquid–liquid partitioning in segregating metabolites based on solvent removal. The DCM fraction showed the highest diversity and intensity of detected metabolites (especially in positive mode), suggesting enrichment of moderately polar metabolites (mainly ST, LPE, LPC, LDGCC, and PC) in both subsets. The BuOH fraction also retained several polar and amphiphilic compounds (e.g., LPI, LPA), some overlapping with those in the DCM fraction (ST, LPE, PC).

In contrast, the Hex fraction exhibited a more restricted profile, enriched in a narrower set of non-polar metabolites (fatty acids, terpenoids, and miscellaneous). The parent MeOH extract exhibited an unfractionated chemical profile, characterized by intermediate levels of many annotated metabolites, and served as a baseline for comparative analysis. This profile likely reflects the presence of residual compounds (e.g., PE, PC) that were not entirely removed during the partitioning process, consistent with its role as the original matrix encompassing a broader diversity and potentially higher abundance of metabolites. Consequently, the clustering patterns and differential distribution confirm that solvent-guided fractionation effectively separated metabolites according to their physicochemical properties. Notably, the BuOH and DCM fractions retained a higher abundance of structurally diverse metabolites, supporting their potential role in the observed biological activities and underscoring their relevance for pharmacological investigation.

Partial Least Squares Discriminant Analysis (PLS-DA) was employed to assess the metabolic differences among the MeOH extract and its derived solvent fractions. As shown in Figure 3, the PLS-DA score plots clearly differentiate the samples based on their chemical profiles under both negative (Figure 3A) and positive (Figure 3B) ionization modes. In the negative ionization mode (Figure 3A), the first two components explained 75.2% and 16.7% of the total variance, respectively. The score plot reveals a distinct clustering of all four extract/fraction types, indicating that each extract/fraction harbors a unique metabolite composition. The BuOH and DCM fractions form separate, tight clusters, suggesting well-defined chemical profiles enriched in polar and moderately polar compounds, respectively. The Hex fraction, dominated by non-polar metabolites, is clearly separated along Component 1. Meanwhile, the MeOH extract occupies a unique position between the fractions, reflecting its broader chemical diversity as the parent extract.

 doi:10.20944/preprints202505.1052.v1

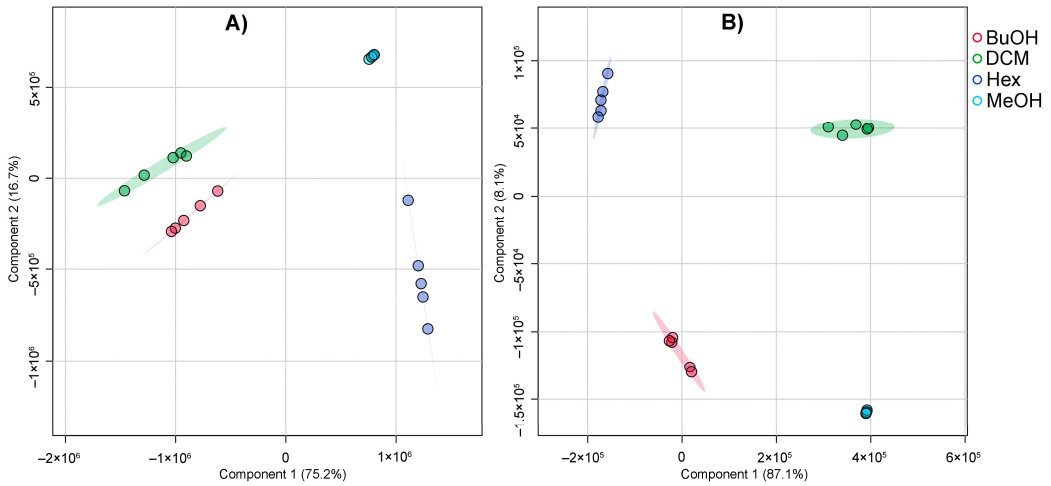

Figure 3. PLS-DA score plots generated from the UHPLC-QTOF-MS datasets. Panel (A) corresponds to the negative ionization mode, while panel (B) corresponds to the positive ionization mode. Each point represents an individual sample from the methanolic extract (MeOH) and its fractions: hexane (Hex), dichloromethane (DCM), and butanol (BuOH). Colored ellipses indicate 95% confidence regions for each group. The percentage of variance explained by each principal component is indicated on the axes.

In the positive ionization mode (Figure 3B), the first two components account for 87.1% and 8.1% of the variance, indicating strong discriminative power of the model. As in the negative mode, the extract/fractions form well-separated clusters with minimal overlap. Again, the BuOH and DCM fractions show strong clustering, highlighting their compositional consistency. The Hex fraction appears more distinct in this mode, and the MeOH extract is again positioned between the extremes, further supporting its role as a chemically rich and heterogeneous matrix. The PLS-DA-derived outcome demonstrated that solvent partitioning effectively segregated metabolite classes based on their polarity and ionization properties. The clear separation among extract/fraction types reinforces the utility of this approach in enriching and distinguishing specialized metabolite subsets for further bioactivity evaluation.

To identify the metabolites driving the separation observed in the PLS-DA score plots, the corresponding loadings plots (Figure 4) were analyzed for both negative (Panel A) and positive (Panel B) ionization datasets. The compounds displayed represent the top contributors (highest loadings on component 1) to the discriminative power of the model. In negative ion mode (Figure 4A), lysophosphatidylinositol (LPI 21:0:1) and several lysophosphatidylethanolamines (LPEs), such as LPE 22:4 and LPE 22:5, were among the most influential compounds. Sulfated sterols (e.g., ST 29:1;O;S and ST 27:1;O;S) also exhibited strong discriminative contributions. The associated heatmap reveals distinct patterns of metabolite distribution across extract/fractions, e.g., sulfated sterols were particularly enriched in the DCM and Hex fractions, whereas LPEs showed higher abundance in BuOH and MeOH, reflecting the polarity-dependent partitioning of these lipids.

 doi:10.20944/preprints202505.1052.v1

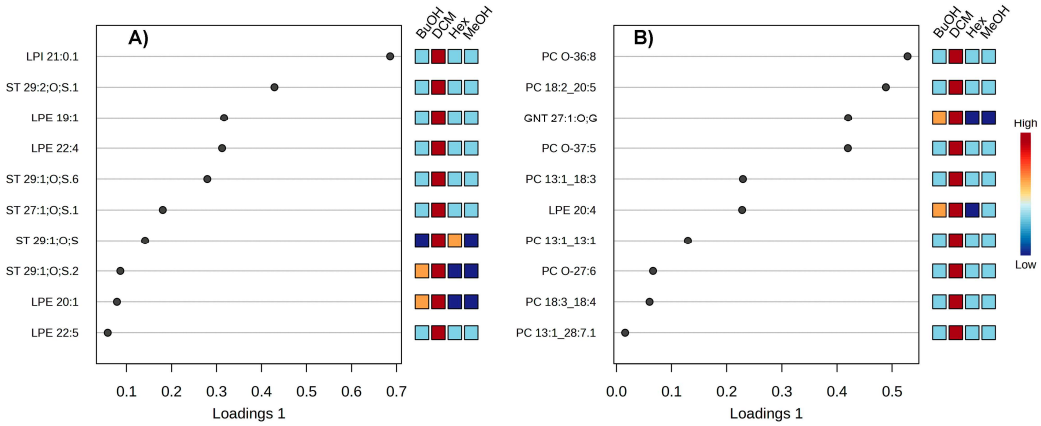

Figure 4. PLS-DA loadings plots displaying the top discriminant metabolites. (A) Metabolites contributing most to sample separation under negative ionization mode. (B) Metabolites contributing most under positive ionization mode. Loadings on component 1 are shown on the x-axis. Heatmaps indicate the relative abundance of each metabolite across the four animal-derived mixtures (BuOH, DCM, Hex, MeOH), with a red-to-blue color scale representing high to low abundance.

In positive ion mode (Figure 4B), discriminant features included several phosphatidylcholines (PCs), such as PC_O-36:8, PC_18:3_18:4, and PC 13:1_28:7:1, along with LPE 20:4 and a glycosylated alkyl-substituted nor-terpenoid (GNT 21:1;O;G). These metabolites showed strong associations with the BuOH and DCM fractions, with phosphatidylcholines more abundant in DCM and BuOH fractions, consistent with their intermediate polarity. Notably, the MeOH extract exhibited moderate levels for most metabolites, underscoring its broad and unspecific metabolite composition as the parent matrix. Collectively, these findings highlight the selective enrichment of lipid subclasses in each solvent fraction. Sulfated sterols and PCs play a pivotal role in differentiating the extract/fractions, supporting the efficiency of the partitioning strategy to segregate bioactive lipid species and providing a chemical rationale for targeted downstream bioactivity assays.

On the other hand, the distribution of STs across the solvent fractions revealed distinct patterns according to ionization mode and fraction polarity. Under negative ionization, ST compounds were particularly enriched in the butanol (BuOH) and dichloromethane (DCM) fractions, accounting for 36.52% and 17.46% of the total metabolite content, respectively. A lower proportion was detected in the Hex fraction (2.16%), while STs were observed at very low abundance in the methanol (MeOH) fraction. In contrast, the positive ionization mode revealed that PCs were the predominant lipid class detected, with their relative abundance varying across extract/fractions: 10.64% in DCM, 5.88% in BuOH, 4.82% in Hex, and 3.28% in MeOH. These results demonstrate that DCM and BuOH fractions are richer in key specialized metabolites, while the MeOH extract contains lower proportions of both ST and PC families.

2.2. Molecular Networks Based on the Global Natural Products Social Molecular Networking (GNPS)

To explore and connect the UHPLC-MS-based chemical diversity of specialized metabolites present in *I. sp. aff. Badionotus* across fractions, we further analyzed the chemical profiles through the global natural product social (GNPS) molecular networking computational web platform. The generated molecular networks (Figure 5) visually represent the chemical space occupied by specialized metabolites in the four solvent extract/fractions. In both negative (panel A) and positive (panel B) ionization modes, clusters of structurally related metabolites were evident, indicating chemical diversity and specificity across extract/fraction types. Based on mass and fragmentation patterns, molecular networks were then examined. The color distribution within clusters indicated that certain metabolite families are exclusive to specific extract/fractions, while others are shared among two or more solvents, revealing the complementary nature of the fractionation. DCM and BuOH share many chemical features, likely due to overlapping polarity ranges, which might explain

 doi:10.20944/preprints202505.1052.v1

the shared presence of key sterols and lipids. On the other hand, Hex and MeOH show fewer shared nodes, reflecting their extraction of chemically distinct metabolite sets—non-polar lipids in Hex and hydrophilic or polar compounds in MeOH. The network analysis confirms that DCM and BuOH fractions harbor the highest chemical diversity, particularly for bioactive specialized metabolites, while the MeOH and Hex fractions show lower complexity or narrower chemical space coverage. These insights reinforce the importance of using a polarity-gradient extraction strategy to capture the broadest spectrum of marine-derived metabolites.

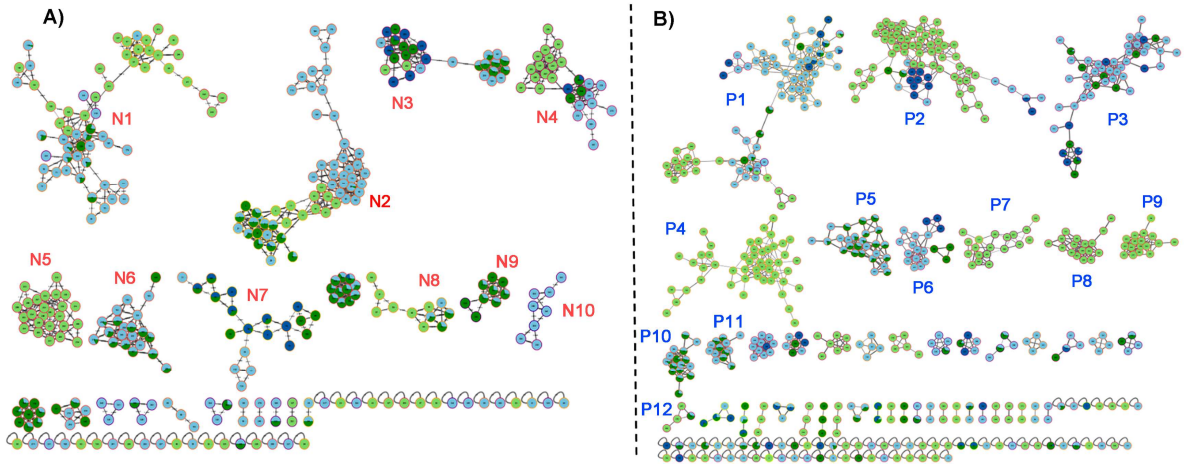

Figure 5. Molecular networks constructed from LC-MS/MS data of *Isostichopus sp. aff. badionotus* extract and fractions. A) Negative mode and B) Positive mode. Each node represents a distinct molecular feature (putative metabolite), and edges indicate structural similarity based on MS/MS fragmentation patterns. The node color reflects the origin of the metabolite across the different solvent extract/fraction (dark blue: methanol, MeOH) and fractions (light blue: dichloromethane, DCM; light green: hexane, Hex; dark green: butanol, BuOH).

The network obtained from the dataset in negative mode (Figure 5A), which is particularly suitable for detecting acidic and sulfated compounds such as sulfated sterols, reveals thirteen densely interconnected clusters predominantly colored in light blue and dark green—indicative of the DCM and BuOH fractions, respectively. These results support the earlier analysis showing a high abundance of sulfated sterols in these two fractions. Hexane fraction (light green) contributes only a few nodes, which agrees with its lower extraction efficiency for polar or ionizable compounds. Metabolites in the methanolic extract (dark blue nodes) are sparsely distributed, highlighting a comparatively lower chemical diversity or ionization efficiency in this mode.

These analyses revealed that cluster N1 involved PE-type compounds with different side chains and substitution patterns, which were mainly identified in the BuOH and DCM fractions, with a higher percentage in the DCM, reaffirming its richness in this lipid-like composition (Figure 6A). This well-defined cluster shows a clear pattern in mass (e.g., m/z 478.3, 490.2, 506.8), consistent with a PE-like lipid core modified by alkyl chain variations.

 doi:10.20944/preprints202505.1052.v1

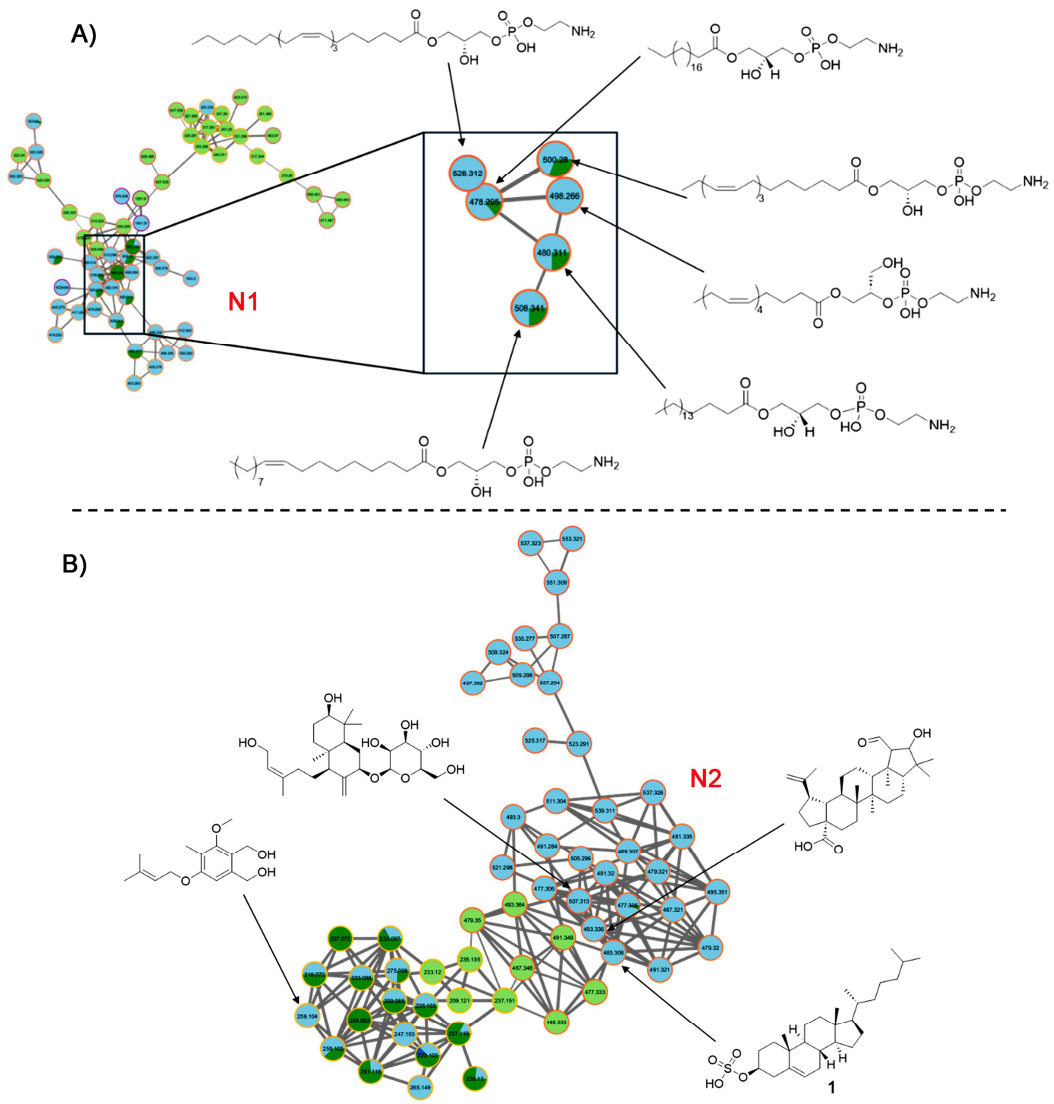

Figure 6. Molecular networks based on GNPS. Identified steroidal compounds and phosphatidylethanolamines (PE). Data analysis in negative mode. Light blue node: DCM fraction; dark green node: BuOH fraction; light green node: Hex fraction.

Similarly, STs were grouped within the same cluster (N2) in their $[M–H]^-$ form (Figure 6B), suggesting structural similarity. This dense network is composed primarily of nodes with light blue and dark green borders, indicating the dominance of metabolites in the DCM and BuOH fractions. The high connectivity suggests a family of structurally related compounds, potentially sterol-like lipids or sulfated triterpenoids, abundant in sea cucumbers and known for their bioactivity. The consistent *m/z* spacing and node proximity suggest sequential modifications such as hydroxylation or sulfation. In this regard, an abundant ST exhibited an MS^2 fragment ion with *m/z* 96.960 ($[M-H]^-$ = 465.3061), matching the structure of cholesterol-3-sulfate (**1**) in the GNPS database, with a cosine score of 0.99. This sulfated sterol **1** has been previously identified in other sea cucumber species and is known as the most abundant sulfated sterol in *Eupentacta fraudatrix*, along with other cholestane derivatives and, to a lesser extent, sulfated stigmastanes [15].

Similarly, metabolite analysis of *Psolus fabricii* revealed the presence of the same sterols, although at significantly lower concentrations [16]. In the case of *Cucumaria frondosa*, it was reported that 51% of the pure fraction of sulfated sterols corresponds to cholesterol sulfate. This evidence supports the identification of compound **1** as cholesterol sulfate. In comparison, the precursor ions of other ST-like compounds showed mass differences of 12 Da ($+CH_2/–H_2$) ($[M–H]^-$ = 477.3062) relative to compound **1**, while others differed by 14 Da ($+CH_2$) ($[M–H]^-$ = 479.3205) and 16 Da ($+CH_2/+H_2$) ($[M–H]^-$ =

 doi:10.20944/preprints202505.1052.v1

481.3525), consistent with campesterol-type sterols. Both cholestane (compound **1**) and campesterol analogs also exhibited hydroxylated variants (+16 Da, +OH). Additional STs displayed a 29 Da increase (+CH_3CH_2) ([M–H]$^-$ = 491.3203) relative to compound **1**, indicative of stigmastane-type sterols. These sulfated sterols have been previously reported in other sea cucumber species.

The remaining identified clusters in the negative ion mode dataset (N3–N10) were associated with various lipid classes and other compound types. Cluster N3 (*m/z* 512–854, [M–H]$^-$) primarily comprised ether-linked phosphatidylethanolamines (PE-O) and lysophosphatidylethanolamines (LPE), while cluster N4 (*m/z* 830–928, [M–H]$^-$) contained ether-linked phosphatidylglycerols (PG-O). Clusters N5 and N6 (*m/z* > 564, [M–H]$^-$) were attributed to lysophosphatidylinositols (LPI) and lysophosphatidylcholines (LPC), respectively. Cluster N7 (*m/z* < 327, [M–H]$^-$) included fatty acids (FA), and cluster N8 (*m/z* < 339, [M–H]$^-$) was dominated by sulfated long-chain hydrocarbons. Cluster N9 (*m/z* < 532, [M–H]$^-$) was assigned to lysoneuroaminophosphatidylethanolamines (LNAPE). Finally, cluster N10 (*m/z* > 1082) comprised high-molecular-weight, yet unidentified, compounds that may represent complex or conjugated lipids.

A different network topology was observed in positive mode (Figure 5B), where neutral and basic compounds such as phosphatidylcholines ionize more efficiently. The formed clusters (P1-P10) were more evenly distributed among the extract/fractions, although DCM (light blue) and BuOH (dark green) still dominate, aligning with their richer and more diverse chemical profiles. Notably, more dark blue nodes (MeOH) appeared in this mode compared to the negative mode, suggesting that the methanolic extract contained metabolites more prone to ionization in positive polarity—likely including polar lipids, peptides, or even glycosides.

Detailed analysis of the molecular network obtained in positive ion mode confirmed a high abundance of [M+H]$^+$ adducts related to phosphatidylcholines (PC), primarily in the DCM and BuOH fractions. Figure 7 displays four relevant clusters (P3, P5, P11, and P12), in which the identified compounds mainly belong to the PC family, with a smaller proportion corresponding to lysophosphatidylcholines (LPC) and phosphatidylinositols (PI).

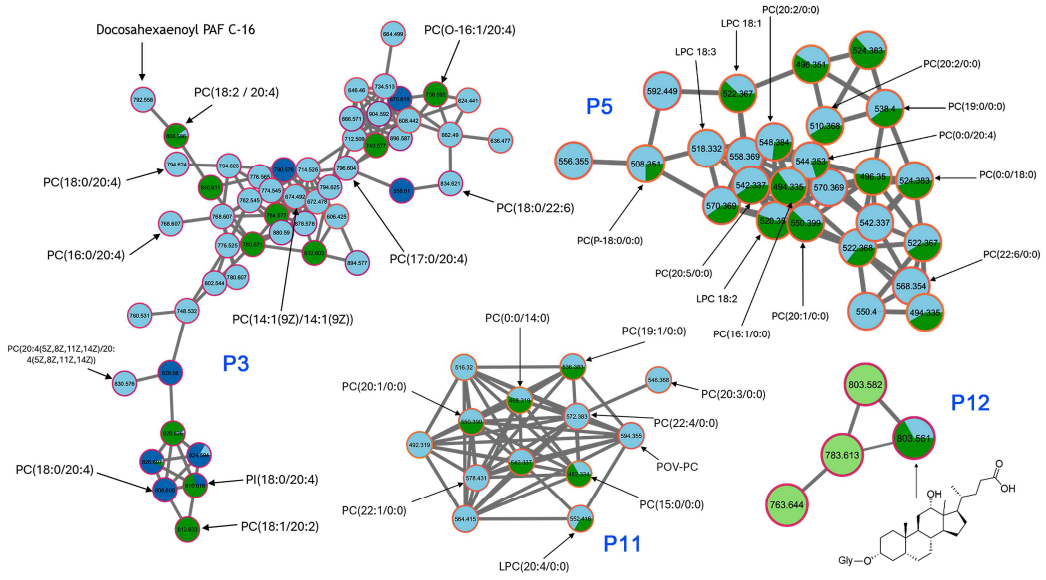

Figure 7. Molecular networks based on GNPS. Data analysis in positive mode. Light blue node: DCM fraction; dark green node: BuOH fraction; light green node: Hex fraction; dark blue node: MeOH extract.

The clusters P3 and P5 were dominated by light blue (DCM) and light green (Hex) node borders. It featured ions in the *m/z* 490–726 range (e.g., 538.4, 544.3, 550.3, 714.55, 716.57, 726.57), which align with mid-polar lipophilic compounds, possibly free fatty acids, oxidized sterols, or monoglycerides. The connectivity suggested a shared core structure modified by alkyl chain variations or oxidations. The Hex preference reflected their moderate polarity, while DCM's enrichment hints at a mix of

 doi:10.20944/preprints202505.1052.v1

amphipathic or lightly functionalized analogs. In addition, the compact and well-structured cluster P11 also included metabolites with strong BuOH and MeOH representation involving phosphocholine-like species. The similarity between nodes and their consistent MS/MS fragmentation supported a common backbone structure with acyl variation. Their solubility in polar solvents again supported their amphipathic nature and roles in membrane dynamics or bioactive signaling. Finally, this sparse mini-cluster contained larger molecules (e.g., m/z 763.6, 803.6) with mixed extract/fraction prevalence but notable BuOH and MeOH dominance. Their high mass range and limited network connectivity suggested the presence of complex glycosylated compounds, such as the annotated steroidal metabolite glycosylated 3,12-dihydroxycholan-24-oic acid (m/z 803.5612, $[M–H]^-$) (Figure 7), which aligns with the well-documented chemical defense mechanisms of sea cucumbers.

2.3. Antibacterial Activity

In this study, the antibacterial activity of the MeOH extract and its fractions DCM, Hex, BuOH from *I.* sp. *aff. badionotus* was evaluated at an initial concentration of 1,000 µg/mL against eight clinically relevant Gram-positive and Gram-negative bacteria. Growth curve analysis revealed that all extract/fractions effectively inhibited bacterial growth by delaying the growth rate of both Gram-positive and Gram-negative strains, with the DCM fraction exhibiting the most pronounced effect (Figure 8).

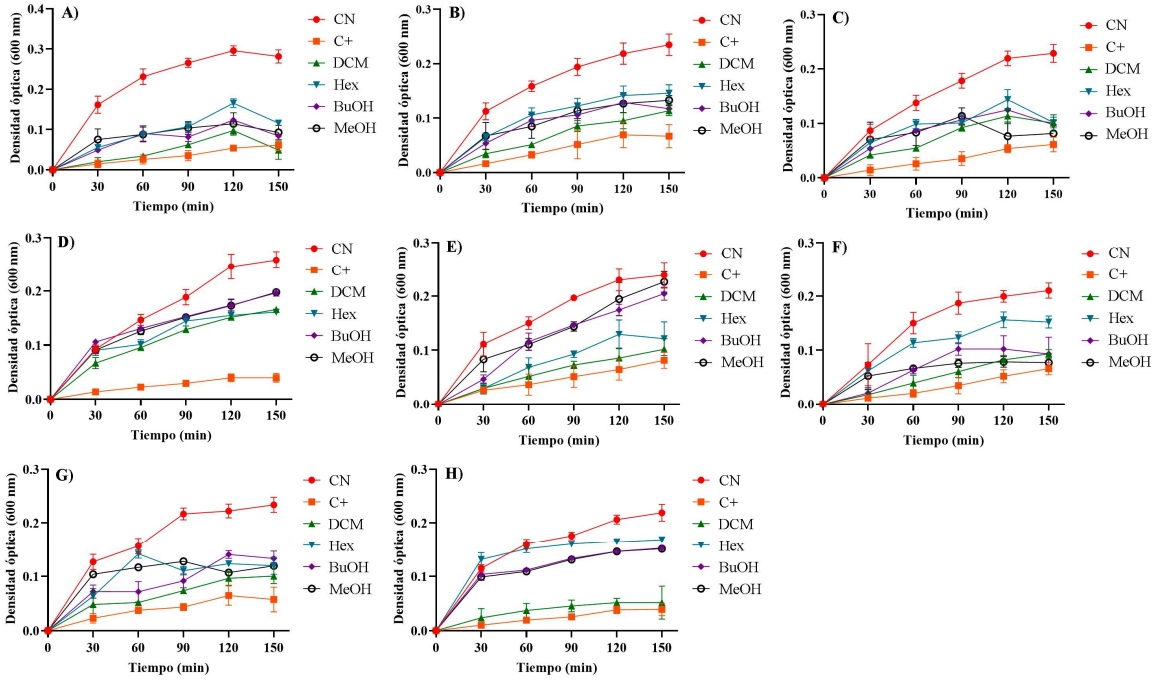

Figure 8. Growth curve of bacteria as a function of exposure to treatments *I.* sp. *aff. badionotus* extract (MeOH) and fractions (Hex, DCm, BuOH) at 1,000 µg/mL against several bacterial strains: *E. coli* (A), *K. pneumoniae* (B), *S. flexneri* (C), *P. aeruginosa* (D), *S. aureus* (E), *B. cereus* (F), *S. epidermidis* (G), and *S. warneri* (H).

The DCM fraction exhibited significant antibacterial activity, particularly against *E. coli* (Figure 9A), with an inhibition rate of 76.5 ± 2.51%, and against several Gram-positive bacteria: *S. aureus* (62.5 ± 3.56%, Figure 9E), *B. cereus* (67.0 ± 2.02%, Figure 9F), *S. epidermidis* (65.5 ± 6.39%, Figure 9G), and *S. warneri* (73.6 ± 6.23%, Figure 9H). These values were statistically higher than those obtained with the other extract/fractions ($p < 0.05$). The Hex and BuOH fractions showed moderate activity, with the highest inhibition also observed against *E. coli*, at 59.8 ± 4.06% and 69.2 ± 4.28%, respectively (Figure 9A). For *K. pneumoniae*, the inhibition values were 38.1 ± 7.27% (Hex) and 46.3 ± 3.00% (BuOH) (Figure 9B); for *S. flexneri*, 45.6 ± 7.64% (Hex) and 42.7 ± 5.18% (BuOH) (Figure 9C); for *S. aureus*, 52.2 ± 3.13%

 doi:10.20944/preprints202505.1052.v1

(Hex) and 24.6 ± 2.54% (BuOH) (Figure 9E); and for *B. cereus*, 50.5 ± 3.48% (Hex) and 58.9 ± 5.78% (BuOH). In contrast, the MeOH extract displayed only mild antibacterial activity.

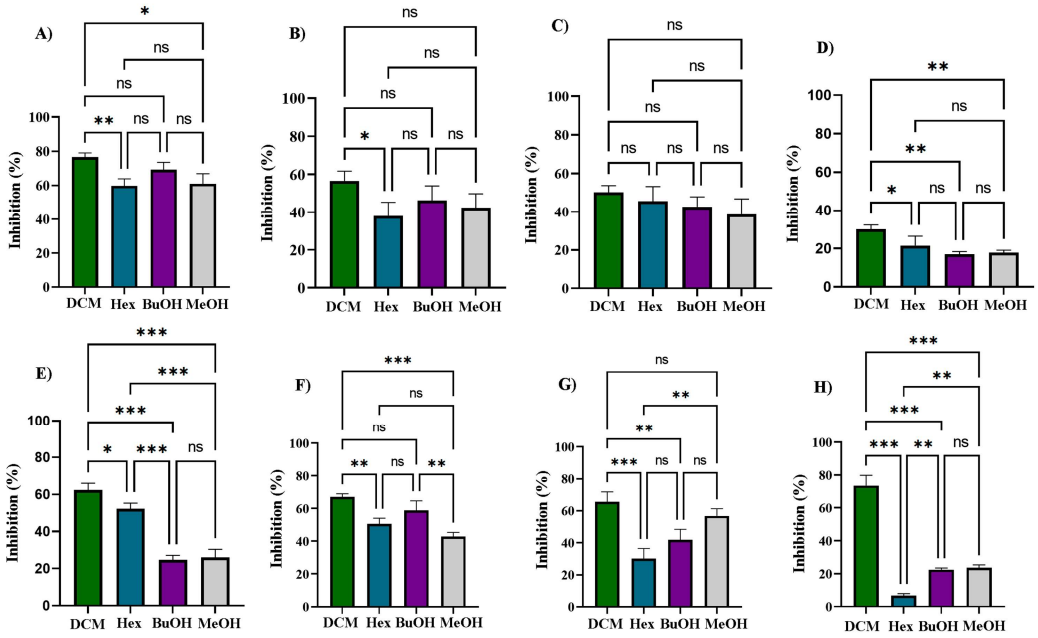

Figure 9. Antibacterial effect of cucumber extract (MeOH) and its derived fractions (Hex, DCM, BuOH) s of *I.* sp. *aff badionotus* evaluated at 1,000 µg/mL against *E. coli* (A), *K. pneumoniae* (B), *S. flexneri* (C), *P. aeruginosa* (D), *S. aureus* (E), *B. cereus* (F), *S. epidermidis* (G) y *S. warneri* (H). In the graph * (0.03), ** (0.002), *** (<0.0001), ns (not significant).

The minimum inhibitory concentration (MIC) of the most active extract/fractions was determined to fall within the 1–1,000 µg/mL range. MIC values were calculated using nonlinear regression, fitting the experimental data to the modified Gompertz equation with GraphPad Prism 9.3 [17]. The calculated MICs aligned with the observed inhibition percentages (Table 1), confirming the superior activity of the DCM fraction. This outcome suggests that the synergistic effects of its constituent compounds offer promising potential for treating infections, especially those caused by Gram-positive bacteria.

Table 1. Minimum inhibitory concentration and R^2 values obtained from fitting the Gompertz equation for MeOH extract and DCM, Hex, and BuOH fractions against the tested bacterial strains.

Extract/ Fractions	MIC (µg/mL) / R^2 (%)							
	E. coli	***K. pneumoniae***	***S. flexneri***	***P. aeruginosa***	***S. aureus***	***B. cereus***	***S. epidermidis***	***S. warneri***
Hex	912 / 95.4	> 1,000 / -	> 1,000 / -	> 1,000 / -	> 1,000 / -	1,000 / -	> 1,000 / -	> 1,000 / -
DCM	540 / 97.2	938 / 93.1	1,000 / -	1,000 / -	724 / 96.7	655 / 94.9	717 / 95.4	579 / 95.7
BuOH	754 / 94.8	> 1,000 / -	> 1,000 / -	> 1,000 / -	> 1,000 / -	930 / 95.2	> 1,000 / -	> 1,000 / -
MeOH	836 / 96.2	> 1,000 / -	> 1,000 / -	> 1,000 / -	> 1,000 / -	> 1,000 / -	988 / 93.3	> 1,000 / -

The observed differences in antibacterial activity may be attributed to structural differences between Gram-positive and Gram-negative bacterial membranes. Gram-positive bacteria possess a simpler cell wall composed primarily of a thick peptidoglycan layer, which facilitates the permeation of bioactive compounds [18]. This increased permeability enhances compound access to critical cellular targets, leading to disruption of essential bacterial processes and, ultimately, cell death [19]. In contrast, Gram-negative bacteria have a more complex cell envelope, consisting of both outer and inner membranes and an intervening layer rich in lipopolysaccharides (LPS). This multilayered structure provides a robust barrier, contributing to resistance against antibiotics, disinfectants, and other lytic agents in the environment [20].

 doi:10.20944/preprints202505.1052.v1

Structurally, the steroidal compounds identified in the most active DCM and BuOH fractions possess both hydrophilic and hydrophobic regions, imparting amphipathic properties. This structural polarity is associated with antimicrobial activity, particularly against Gram-positive bacteria, through mechanisms that include destabilization of membrane integrity and increased permeability. These disruptions lead to membrane rupture and leakage of intracellular contents, ultimately resulting in bacterial death [21,22]. Additionally, these metabolites may interfere with membrane potential and the proton motive force at the mitochondrial level, further compromising bacterial viability [23]. These factors may explain the differential antibacterial effects observed between the DCM fraction and the other extract/fractions tested.

The antibacterial activity demonstrated by the test materials from the sea cucumber *I.* sp. *aff. badionotus* makes a valuable contribution to the field of natural product research. This work supports ongoing efforts to discover potent specialized metabolites from marine sources with activity against clinically relevant pathogens. In recent years, many studies have focused on exploring natural resources due to their diverse array of molecules with antibacterial potential [24,25]. Such research has emphasized mechanisms of action targeting bacterial membrane proteins, efflux pumps, biofilm formation, and quorum sensing—all of which play crucial roles in developing antimicrobial resistance [26]. Natural products may act independently or serve as complementary agents to enhance the efficacy of conventional antibiotic therapies.

3. Materials and Methods

3.1. Collection and Extraction of Sea Cucumber I. sp. aff badionotus Specimens.

Adult specimens of the sea cucumber *Isostichopus* sp. aff. *badionotus* were manually collected from three coastal locations in the Santa Marta Bay, Colombian Caribbean: Rodadero (11°13’22.73” N, 74°13’32.59” W), Airport (11°07’10” N, 74°13’50” W), and Taganga Beach (11°16’04.6” N, 74°11’46.9” W). Immediately after collection, specimens were stored at 4 °C and transported to the laboratory under chilled conditions. Voucher samples were deposited in the Biological Collections of the University of Magdalena (CBUMAG:ECH:00001, CBUMAG:ECH:00002, CBUMAG:ECH:00003).

Tissue animal samples from the pooled specimens were cut into small pieces and frozen at -80 °C for freeze-drying and ground before extraction. A methanolic exhaustive maceration was performed at room temperature for 72 h (3×), and the combined filtrates were concentrated under reduced pressure to obtain the crude methanol extract. This resulting extract was subsequently subjected to sequential liquid-liquid partitioning using solvents of increasing polarity: *n*-hexane (Hex), dichloromethane (DCM), and *n*-butanol (BuOH). Each solvent partitioning was performed in a separatory funnel with equal volumes (1:1, v/v) of the aqueous-methanol residue and the respective organic solvent. The resulting organic phases were individually collected, dried over anhydrous sodium sulfate, filtered, and evaporated under reduced pressure to yield the Hex, DCM, and BuOH fractions used in subsequent bioassays and chemical profiling.

3.2. Biological Assay

3.2.1. Strains

Eight clinically relevant bacterial strains were used to assess the antibacterial activity of the *Isostichopus* sp. aff. *badionotus* fractions. These included four Gram-negative strains: *Escherichia coli* ATCC 25922, *Klebsiella pneumoniae* ATCC 1705, *Shigella flexneri* ATCC 12022, and *Pseudomonas aeruginosa* ATCC 10195, and four Gram-positive strains: *Staphylococcus aureus* ATCC 6538, *Bacillus cereus* ATCC 11778, *Staphylococcus epidermidis*, and *Staphylococcus warneri*. All strains were cultured in Mueller–Hinton broth (MHB) and maintained under standard laboratory conditions.

 doi:10.20944/preprints202505.1052.v1

3.2.2. Antibacterial Activity Assay

The antibacterial activity of each solvent-partitioned fraction was determined using the broth microdilution method according to the Clinical and Laboratory Standards Institute (CLSI) guidelines (version 2022). Briefly, 100 µL of each fraction solution (dissolved in 1% DMSO) was mixed with 100 µL of bacterial suspension (adjusted to OD_{600} = 0.05) in 96-well microplates, yielding a final testing concentration of 1,000 µg/mL per well. Gentamicin (40 µg/mL) served as a positive control, while 1% DMSO and uninoculated broth were included as negative and sterility controls, respectively. Plates were incubated at 37 °C for 150 minutes, and bacterial growth was monitored by measuring the optical density at 600 nm every 30 minutes [27]. The percentage of bacterial inhibition was calculated according to the following equation:

$$\text{Inhibition (\%)} = \frac{DO_{CN} - DO_T}{DO_{CN}} \times 100$$

Where DO_{CN}, corresponds to the optical density of the negative control and DO_T to the optical density of the treatments. Additionally, the minimum inhibitory concentration (MIC) of each fraction was determined based on the lowest concentration that inhibited visible bacterial growth.

3.2.3. Statistical Analysis

Each experimental condition was performed in triplicate, with four technical replicates per treatment (n = 12). Data reproducibility was assessed using Levene's test for homogeneity of variances (coefficient of variation, CV < 20%). Statistical significance among groups was evaluated using one-way analysis of variance (ANOVA) followed by Tukey's post hoc test ($p < 0.05$). All statistical analyses were carried out using GraphPad Prism software, version 9.3.0 (GraphPad Software, San Diego, CA, USA).

3.3. UHPLC-HRMS-Bases Analysis

The extract and its fractions were subjected to metabolic profiling using ultra-high-performance liquid chromatography coupled with high-resolution mass spectrometry (UHPLC-HRMS) to understand better and relate the observed biological activity. Dried extract/fractions were subjected to chemical characterization using UHPLC coupled with Quadrupole Time-of-Flight Mass Spectrometry (UHPLC-QTOF-MS; Compact QTOF MS + Elute UHPLC, Bruker Daltonik GmbH, Bremen, Germany). The MeOH extract and its Hex, DCM, BuOH fractions were dissolved and transferred into HPLC-grade vials. Chromatographic separation was performed on a Kinetex C18 column (maintained at 40 °C), using 0.1% formic acid in water (solvent A) and 0.1% formic acid in 90% acetonitrile (solvent B) as the mobile phases. A 5 µL injection volume was used, with a flow rate of 0.5 mL/min. The gradient elution program was as follows: 0 min, 88% A; 12.5 min, 70% A; 14.5 min, 40% A; 19 min, 88% A, for a total run time of 19 minutes. Mass spectrometric data were acquired in both negative and positive electrospray ionization (ESI) modes over an m/z range of 120–1800. The source parameters were set as follows: spray voltage, 3 kV; sheath gas, 30 psi; auxiliary gas, 13 psi; capillary temperature, 350 °C; S-Lens RF level, 50; and heater temperature, 150 °C. Compound annotation was achieved by integrating high-resolution monoisotopic mass measurements, MS/MS fragmentation patterns, and chromatographic retention times. These data were cross-referenced with established spectral libraries, including MS-DIAL, MassBank of North America (MoNA), and LipidBlast, to ensure accurate annotation of the detected metabolites.

3.4. Molecular Networks

Raw chromatographic data were converted to mzXML format and uploaded to the Global Natural Products Social Molecular Networking (GNPS) platform (https://gnps.ucsd.edu/) for dereplication and construction of molecular networks [28]. Spectral clustering was based on cosine similarity scores and compared with public GNPS libraries to facilitate metabolite annotation. Molecular networking allowed the visualization of structurally related compounds and the putative

 doi:10.20944/preprints202505.1052.v1

identification of bioactive metabolites, contributing to the observed antibacterial effects. Data processing and compound annotation were performed using MetaboScape 4.0 software (Bruker), referencing the MassBank of North America (MoNA) spectral library.

4. Conclusions

This study underscores the promising potential of marine-derived natural products, particularly those from sea cucumbers, as valuable sources of antibacterial agents. Extract and fractions from *Isostichopus* sp. aff. *badionotus*— particularly the DCM fraction—exhibited notable antibacterial activity against both Gram-positive and Gram-negative bacteria. This bioactivity is primarily attributed to the presence of sulfated sterols, which were found in high abundance in the DCM fraction. Complementary metabolomic profiling revealed a chemically diverse set of specialized metabolites, including sulfated sterols and phosphatidylcholines, that may synergistically contribute to the observed antimicrobial effects. These results highlight the relevance of marine invertebrates as underexplored reservoirs of bioactive compounds and support their continued investigation as alternative solutions to address the global threat of antibiotic resistance. Further bioactivity-guided fractionation and mechanistic studies are warranted to fully assess their therapeutic potential.

Author Contributions: Conceptualization, Y.AR-N, M.T-M, M.B and A.R-F; investigation, Y.AR-N, M.T-M, M.B, E.C.-B., and F.E-A.; writing-original draft preparation, Y.AR-N, M.T-M, M.B, and F.E-A. writing—review and editing, Y.AR-N, E.C.-B., M.T-M; All authors have read and agreed to the published version of the manuscript.

Funding: This research was funded by Vicerrectoría de Investigación at Universidad del Magdalena.

Institutional Review Board Statement: Not applicable.

Informed Consent Statement: Not applicable.

Data Availability Statement: Data generated or analyzed in this study are included in this article.

Acknowledgments: Y.A.R-N thanks for Project FONDECYT N°11241068. M.B. thanks for the FONDECYT project N° 3220756. M.T-M thanks Ministerio de Ciencias Tecnología e Investigación de Colombia. E.C.-B. thanks Universidad Militar Nueva Granada (Project EXT-CIAS-3854).

Conflicts of Interest: The authors declare no conflicts of interest.

References

1. Urban-Chmiel, R.; Marek, A.; Stępień-Pyśniak, D.; Wieczorek, K.; Dec, M.; Nowaczek, A.; Osek, J. Antibiotic Resistance in Bacteria—A Review. *Antibiotics* 2022, *11*, 1079, doi:10.3390/ANTIBIOTICS11081079/S1.
2. Banday, A.H.; Azha, N. ul; Farooq, R.; Sheikh, S.A.; Ganie, M.A.; Parray, M.N.; Mushtaq, H.; Hameed, I.; Lone, M.A. Exploring the Potential of Marine Natural Products in Drug Development: A Comprehensive Review. *Phytochem Lett* 2024, *59*, 124–135, doi:10.1016/J.PHYTOL.2024.01.001.
3. Mercier, A.; Gebruk, A.; Kremenetskaia, A.; Hamel, J.F. An Overview of Taxonomic and Morphological Diversity in Sea Cucumbers (Holothuroidea: Echinodermata). *The World of Sea Cucumbers: Challenges, Advances, and Innovations* 2024, 3–15, doi:10.1016/B978-0-323-95377-1.00001-1.
4. Rasyid, A.; Putra, M.Y.; Yasman Antibacterial and Antioxidant Activity of Sea Cucumber Extracts Collected from Lampung Waters, Indonesia. *Kuwait Journal of Science* 2023, *50*, 615–621, doi:10.1016/J.KJS.2023.03.012.
5. Nugroho, A.; Harahap, I.A.; Ardiansyah, A.; Bayu, A.; Rasyid, A.; Murniasih, T.; Setyastuti, A.; Putra, M.Y. Antioxidant and Antibacterial Activities in 21 Species of Indonesian Sea Cucumbers. *J Food Sci Technol* 2022, *59*, 239–248, doi:10.1007/S13197-021-05007-6.
6. Wargasetia, T.L.; Ratnawati, H.; Widodo, N.; Widyananda, M.H. Antioxidant and Anti-Inflammatory Activity of Sea Cucumber (Holothuria Scabra) Active Compounds against KEAP1 and INOS Protein. *Bioinform Biol Insights* 2023, *17*, doi:10.1177/11779322221149613.

 doi:10.20944/preprints202505.1052.v1

7. Feng, J.; Wang, H.; Luo, X.; Zhang, L.; Zhou, P. Identification and Molecular Mechanism of the Anti-Inflammatory Effect of Sea Cucumber Peptides: Network Pharmacology, Molecular Docking and Animal Experiments. *Int J Biol Macromol* 2024, *279*, 134958, doi:10.1016/J.IJBIOMAC.2024.134958.
8. Aminin, D.L.; Menchinskaya, E.S.; Pisliagin, E.A.; Silchenko, A.S.; Avilov, S.A.; Kalinin, V.I. Anticancer Activity of Sea Cucumber Triterpene Glycosides. *Marine Drugs 2015, Vol. 13, Pages 1202-1223* 2015, *13*, 1202–1223, doi:10.3390/MD13031202.
9. Janakiram, N.B.; Mohammed, A.; Rao, C. V. Sea Cucumbers Metabolites as Potent Anticancer Agents. *Marine Drugs 2015, Vol. 13, Pages 2909-2923* 2015, *13*, 2909–2923, doi:10.3390/MD13052909.
10. Vishkaei, M.S.; Ebrahimpour, A.; Abdul-Hamid, A.; Ismail, A.; Saari, N. Angiotensin-I Converting Enzyme (ACE) Inhibitory and Antihypertensive Effect of Protein Hydrolysate from Actinopyga Lecanora (Sea Cucumber) in Rats. *Marine Drugs 2016, Vol. 14, Page 176* 2016, *14*, 176, doi:10.3390/MD14100176.
11. Mohamadzadeasl, A.; Khodabandeh, S. Antioxidant and Anti-Hypertension Activities of Protein Hydrolysate from Sea Cucumber, Holothuria Parva Using Enzymatic Hydrolysis. 2023, doi:10.21203/RS.3.RS-2882086/V1.
12. Kiani, N.; Heidari, B.; Rassa, M.; Kadkhodazadeh, M.; Heidari, B. Antibacterial Activity of the Body Wall Extracts of Sea Cucumber (Invertebrata; Echinodermata) on Infectious Oral Streptococci. *J Basic Clin Physiol Pharmacol* 2014, *25*, 367–373, doi:10.1515/JBCPP-2013-0010.
13. Jiang, J.; Zhou, Z.; Dong, Y.; Cong, C.; Guan, X.; Wang, B.; Chen, Z.; Jiang, B.; Yang, A.; Gao, S.; et al. In Vitro Antibacterial Analysis of Phenoloxidase Reaction Products from the Sea Cucumber Apostichopus Japonicus. *Fish Shellfish Immunol* 2014, *39*, 458–463, doi:10.1016/J.FSI.2014.06.002.
14. Mohammadi Movahed, M.; Hosseini, S.A.; Akbary, P.; Hajimoradloo, A.; Hedayati, S.A.A. Antibacterial Activity of Muscle Wall Extracts of Sea Cucumber (Stichopus Horrens) from Chabahar Coastal Area, Iran, against Pathogenic Bacteria in Rainbow Trout (Oncorhynchus Mykiss). *J Appl Anim Res* 2021, *49*, 340–346, doi:10.1080/09712119.2021.1967161.
15. Makarieva, T.N.; Stonik, V.A.; Kapustina, I.I.; Boguslavsky, V.M.; Dmitrenoik, A.S.; Kalinin, V.I.; Cordeiro, M.L.; Djerassi, C. Biosynthetic Studies of Marine Lipids. 42. Biosynthesis of Steroid and Triterpenoid Metabolites in the Sea Cucumber Eupentacta Fraudatrix. *Steroids* 1993, *58*, 508–517, doi:10.1016/0039-128X(93)90026-J.
16. Goad, L.J.; Garneau, F.X.; Simard, J.L.; Apsimon, J.W.; Girard, M. Composition of the Free, Esterified and Sulphated Sterols of the Sea Cucumber Psolus Fabricii. *Comparative Biochemistry and Physiology Part B: Comparative Biochemistry* 1986, *84*, 189–196, doi:10.1016/0305-0491(86)90204-X.
17. Hammond, R.J.H.; Falconer, K.; Powell, T.; Bowness, R.; Gillespie, S.H. A Simple Label-Free Method Reveals Bacterial Growth Dynamics and Antibiotic Action in Real-Time. *Scientific Reports 2022 12:1* 2022, *12*, 1–11, doi:10.1038/s41598-022-22671-6.
18. Gilmore, M.C.; Ritzl-Rinkenberger, B.; Cava, F. An Updated Toolkit for Exploring Bacterial Cell Wall Structure and Dynamics. *Fac Rev* 2021, *10*, 14, doi:10.12703/R/10-14.
19. Garde, S.; Chodisetti, P.K.; Reddy, M. Peptidoglycan: Structure, Synthesis, and Regulation. *EcoSal Plus* 2021, *9*, doi:10.1128/ECOSALPLUS.ESP-0010-2020/ASSET/489D3FE6-0F6C-4920-B996-B48938850558/ASSETS/GRAPHIC/ESP-0010-2020_FIG_005.GIF.
20. Pajerski, W.; Ochonska, D.; Brzychczy-Wloch, M.; Indyka, P.; Jarosz, M.; Golda-Cepa, M.; Sojka, Z.; Kotarba, A. Attachment Efficiency of Gold Nanoparticles by Gram-Positive and Gram-Negative Bacterial Strains Governed by Surface Charges. *Journal of Nanoparticle Research* 2019, *21*, doi:10.1007/S11051-019-4617-Z.
21. Bacho, M.; Artigas, V.; Araya-Contreras, T.; Bittner, M.; Escobar, C.A.; Fuentealba, M.; Becerra, J.; Fajardo, V.; San-Martín, A. Synthesis, Characterisation, Crystal Structure and Antimicrobial Evaluation of Novel 6-Alkoxyergosta-4,6,8(14),22-Tetraen-3-One Derived from Natural Ergosta-5,7,22-Trien-3β-Ol. *Nat Prod Res* 2023, *37*, 16–23, doi:10.1080/14786419.2021.1946534.
22. Alhanout, K.; Malesinki, S.; Vidal, N.; Peyrot, V.; Rolain, J.M.; Brunel, J.M. New Insights into the Antibacterial Mechanism of Action of Squalamine. *Journal of Antimicrobial Chemotherapy* 2010, *65*, 1688–1693, doi:10.1093/JAC/DKQ213.

 doi:10.20944/preprints202505.1052.v1

23. Sikkema, J.; De Bont, J.A.M.; Poolman, B. Mechanisms of Membrane Toxicity of Hydrocarbons. *Microbiol Rev* 1995, *59*, 201–222, doi:10.1128/mmbr.59.2.201-222.1995.
24. Khare, T.; Anand, U.; Dey, A.; Assaraf, Y.G.; Chen, Z.S.; Liu, Z.; Kumar, V. Exploring Phytochemicals for Combating Antibiotic Resistance in Microbial Pathogens. *Front Pharmacol* 2021, *12*, doi:10.3389/FPHAR.2021.720726.
25. Suganya, T.; Packiavathy, I.A.S.V.; Aseervatham, G.S.B.; Carmona, A.; Rashmi, V.; Mariappan, S.; Devi, N.R.; Ananth, D.A. Tackling Multiple-Drug-Resistant Bacteria With Conventional and Complex Phytochemicals. *Front Cell Infect Microbiol* 2022, *12*, doi:10.3389/FCIMB.2022.883839.
26. Contreras-Gómez, M.J.; Martinez, J.R.W.; Rivas, L.; Riquelme-Neira, R.; Ugalde, J.A.; Wozniak, A.; García, P.; Munita, J.M.; Olivares-Pacheco, J.; Alcalde-Rico, M. Role of the Multi-Drug Efflux Systems on the Baseline Susceptibility to Ceftazidime/Avibactam and Ceftolozane/Tazobactam in Clinical Isolates of Non-Carbapenemase-Producing Carbapenem-Resistant Pseudomonas Aeruginosa. *Front Pharmacol* 2022, *13*, 1007162, doi:10.3389/FPHAR.2022.1007162/BIBTEX.
27. Espitia-Almeida, F.; Valle-Molinares, R.; Navarro Quiroz, E.; Pacheco-Londoño, L.C.; Galán-Freyle, N.J. Photodynamic Antimicrobial Activity of a Novel 5,10,15,20-Tetrakis (4-Ethylphenyl) Porphyrin against Clinically Important Bacteria. *Pharmaceuticals 2023, Vol. 16, Page 1059* 2023, *16*, 1059, doi:10.3390/PH16081059.
28. Wang, M.; Carver, J.J.; Phelan, V. V.; Sanchez, L.M.; Garg, N.; Peng, Y.; Nguyen, D.D.; Watrous, J.; Kapono, C.A.; Luzzatto-Knaan, T.; et al. Sharing and Community Curation of Mass Spectrometry Data with Global Natural Products Social Molecular Networking. *Nature Biotechnology 2016 34:8* 2016, *34*, 828–837, doi:10.1038/nbt.3597.